OCEANOGRAPHY

Seismic crustal imaging using fin whale songs

Václav M. Kuna[1,2]* and John L. Nábělek[1]

Fin whale calls are among the strongest animal vocalizations that are detectable over great distances in the oceans. We analyze fin whale songs recorded at ocean-bottom seismometers in the northeast Pacific Ocean and show that in addition to the waterborne signal, the song recordings also contain signals reflected and refracted from crustal interfaces beneath the stations. With these data, we constrain the thickness and seismic velocity of the oceanic sediment and basaltic basement and the *P*-wave velocity of the gabbroic lower crust beneath and around the ocean bottom seismic stations. The abundant and globally available fin whale calls may be used to complement seismic studies in situations where conventional air-gun surveys are not available.

The fin whale (*Balaenoptera physalus*) is an endangered (*1*) cetacean that populates global oceans from polar regions to equatorial waters (*2*), with an estimated population of 100,000 (*3*). Fin whale vocalizations are among the strongest animal calls in the ocean (*4*–*6*). Reaching up to 189 dB (1 μPa at 1 m) (*5*, *6*), the source levels are comparable to those of noise produced by large ships (*4*). The calls can be monitored hundreds of miles away from the source (*4*), enabling studies of whale behavior, abundance, distribution, and migration patterns (*7*–*13*).

Fin whale vocalizations include short, 1-s calls with a dominant frequency of around 20 Hz (*14*). Calls are characterized by a sinusoidal, downward frequency-sweeping signal, with about a 5-Hz drop in frequency over the duration of the call (*7*). These calls repeat every 7 to 40 s (*7*, *15*, *16*), forming songs that last up to tens of hours, with short interruptions about every 15 min when the whale surfaces (*7*) (fig. S1). The songs may be composed of a single repeating call but often consist of two or three alternating calls with different downward-sweeping character (*16*) (Fig. 1, A and B, and figs. S2 and S3). Ocean-bottom seismometer (OBS) stations deployed for earthquake monitoring are commonly configured to record vibrations of 50 Hz and lower and often capture vocalizations of whales with low-frequency calls, including those of fin whales (*8*, *11*–*13*). We show that the fin whale calls recorded at OBS stations contain, in addition to waterborne energy, signals reflected and refracted from crustal interfaces beneath the station that can be used for seismic imaging of the oceanic crust.

From 2012 to 2013, a network of 54 OBS stations was deployed in the northeast Pacific Ocean to monitor the seismicity of the Blanco transform fault (*17*, *18*). Besides fault seismicity, OBS stations recorded numerous fin whale songs (fig. S4), which often lasted up to 10 hours. We analyzed fin whale songs recorded at the BS080, BS100, and BS110 stations of the OBS network (Fig. 2). The stations were deployed 20 to 40 km north of the Blanco fault at a depth of about 3000 m, in a flat region without a substantial variation in bathymetry. The sites were 270 to 330 km from the Juan de Fuca spreading ridge, which corresponds to a crustal age of about 5 million to 7 million years (*19*). The three OBS stations were equipped with short-period, three-component seismic sensors and differential pressure gauges, recording data streams at the rate of 100 samples per second (*20*).

We analyzed a total of six songs, each formed by vocalizations of a single whale. Two were recorded in October and November 2012 at BS080, two in September 2012 and September 2013 at BS100, and two in September 2012 and May 2013 at BS110 (Fig. 2, fig. S5, and table S1). The song durations range from 2.5 to 4.9 hours, during which time the whales covered distances between 16 and 38 km with mean cruising speeds between 2.2 and 5.6 knots (4.1 to 10.3 km hour^{-1}). The whales traveled on oblique paths around the stations, swimming from as far as 19 km from the stations to as close as 700 m. The songs primarily consisted of calls of two distinct types: a downward-sweeping call with dominant frequencies between 25 and 20 Hz and a lower-pitch call that dropped in frequency from 20 to 15 Hz (Fig. 1A and figs. S2 and S3). Owing to lower background noise levels in the higher-frequency range, we used only the higher-pitch calls. The songs contained 212 to 593 calls, with intercall times between 30 and 40 s (fig. S5B). To enhance the useful signal, we filtered the data using a tapered Butterworth bandpass filter with a passband from 21 to 25 Hz.

We determined the distance between the whale (i.e., the source) and the station from the difference in arrival times of the direct water wave and the waterborne multiple, which is the reflected water wave that bounces between the seafloor and the sea surface before reaching the station [Fig. 1, C and E; (*20*)]. We assumed that the whales swam at a depth of 10 m, given that fin whales typically call while swimming at depths between 0 and 20 m (*21*). With a depth range of 10 ± 10 m, the estimated uncertainty of the source-station distance at 20 km is 30 m. To find the actual whale swim path, we calculated the whale location by combining the distance and the azimuth between the whale and the station. We determined the station-source azimuth from the directivity of the direct water wave that aims toward the source [Fig. 1D; (*20*)]. The final travel path was smoothed with a moving average filter based on reasonable assumptions that the whale trajectory is expected to be relatively smooth and the cruising velocity steady. Changing seafloor bathymetry may influence the source-station distance determination, and we correct for this effect by using an iterative location method (*20*). However, the bathymetry around the studied stations is generally very flat.

When a fin whale call impinges on the ocean bottom, part of the call energy is transmitted in the ground as a seismic wave. The seismic wave travels through the oceanic crust, where it is reflected and refracted by layers within the crust. When recorded at an OBS station, it enables us to estimate the crustal structure. To show arrivals of individual seismic phases, we organized the whale calls into the receiver gathers. A receiver gather represents a collection of individual whale calls (i.e., seismic traces) displayed according to the distance between the whale and the station at the time of the call (i.e., source-station offset). Each of the receiver gathers comprises whale calls recorded during one song, which we refer to as a song gather. Individual phase arrivals appear in song gathers as intervals of a relatively high-amplitude signal. With increasing distance, the phases arrive progressively later, a process termed normal moveout (NMO). The accurate medium velocity corrects for the NMO by making phase arrival times equivalent at all distances, which can be used to estimate medium velocity. The seismic phase arrivals are best displayed in song gathers from the vertical seismometer component (Fig. 3). The most prominent arrivals in song gathers are the waterborne waves—the direct wave W(dir) and the reflected (multiple) wave W(mult). In addition to the waterborne waves, we identified four dominant seismic phases belonging to wave reflections and refractions in the basaltic basement (i.e., layer 2) and refractions in the gabbroic lower crust (i.e., layer 3). The best-fitting crustal model for each station (Table 1) was found by regression of arrival times of the individual phases and modeled using a ray-modeling software (*20*, *22*). Despite near-horizontal bathymetry, we observe signal fluctuations and differences in the appearance of waterborne and seismic phases in

[1]College of Earth, Ocean, and Atmospheric Sciences, Oregon State University, Corvallis, OR 97331, USA. [2]Institute of Geophysics of the CAS, 141 31 Prague, Czech Republic.
*Corresponding author. Email: kuna@ig.cas.cz

the individual song gathers at horizontal scales of 200 to 500 m. These differences could be due to scattering from ripples at the sediment surface caused by ocean-bottom currents, heterogeneity in the sediment layering, and rough topography on layer 2.

P-wave reflections from the top of the basement (layer 2) can be identified after the arrival of the direct waterborne wave W(dir) or the waterborne multiple W(mult). The WPbP corresponds to the direct wave reflection and the W(mult)PbP to the waterborne multiple reflection. The basement reflections enable us to calculate the thickness and the *P*-wave velocity of the oceanic sediment, layer 1. When the direct water wave impinges obliquely on the interface between the water and the sediment layer, part of the wave energy is converted to an *S* wave. *S*-wave reflections from layer 2 (WSbS) arrive in the song gather between the waterborne wave arrivals (Fig. 3 and figs. S6 to S8). The WSbS provides an independent estimate of the sediment thickness and constrains the *S*-wave velocity and the Poisson ratio of layer 1. At offsets greater than about 4 km, the *P* wave refracted along the basaltic basement (referred to as WPg) becomes the first arriving phase and constrains the *P*-wave velocity of layer 2 as well as the layer 1 thickness. At offsets greater than about 12 km, the velocity of the WPg phase increases, which indicates the arrival of a *P* wave refracted along the gabbroic lower crust (layer 3). The WPg(L3) enables us to calculate the layer 2 thickness and the *P*-wave velocity of layer 3.

The basaltic basement reflections WPbP and W(mult)PbP are observed at all stations, arriving about 0.5 to 0.7 s after the respective waterborne waves at 2-km source-station offsets (figs. S6 to S8). For longer offsets, the time difference between the reflected phases and the waterborne wave arrivals decreases, indicating faster NMO velocity of the reflected phase arrival. The optimal NMO correction of the W(mult)PbP phase uses a velocity between 1.53 and 1.56 km s^{-1}, which indicates that the *P*-wave velocity in the sediment layer is between 1.9 and 2.2 km s^{-1} (Fig. 3D and fig. S9). The difference between the phase travel time of W(mult)PbP and W(mult) suggests a total sediment thickness of about 500, 650, and 400 m at BS080, BS100, and BS110, respectively, with an estimated uncertainty of about 30 to 40 m (Table 1 and figs. S10 to S12).

Appearing at short offsets, about 1.5 to 2 s after the W(dir) at 2 km, the *S*-wave basement reflection WSbS is a dominant phase on all song gathers. The NMO of the reflected WSbS phase (Fig. 3E) suggests that the *S*-wave velocity of the oceanic sediment layer is roughly 0.6 km s^{-1}. The sediment Poisson ratio is in the range of 0.44 to 0.46, and the ratio of *P*- to *S*-wave velocity (v_p/v_s) ratio is between 3.2 and 3.7. The WSbS phase arrivals are consistent with the sediment thickness determined from the W(mult)PbP phase.

The WPg phase, representing the *P* wave refracted along the basaltic basement (layer 2), indicates a basaltic basement velocity between 5.5 and 5.9 km s^{-1} at all stations (figs. S10 to S12), with an uncertainty of about 0.2 km s^{-1}. Differing slopes of WPg recorded at song gathers at opposite sides of a station indicate that the top of layer 2 may be dipping. The effect of the offset uncertainty on the model

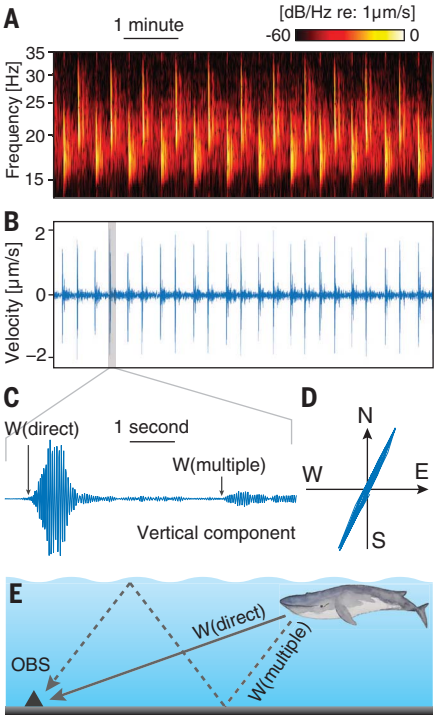

Fig. 1. Characteristics of fin whale vocalizations. (**A**) Spectrogram of a 7-min section of an unfiltered fin whale song, recorded by the vertical seismometer component at the station BS080 (November 2012 whale song; see Fig. 2 for location). re, relative to. (**B**) Song section in the time domain. (**C**) Magnification of a single fin whale call. Waterborne wave arrivals are denoted with arrows. (**D**) An example of a direct-wave arrival recorded at the station's horizonal components, showing polarization along the azimuth to the whale. (**E**) A sketch illustrating travel paths of waterborne phases used for estimating the distance to the whale.

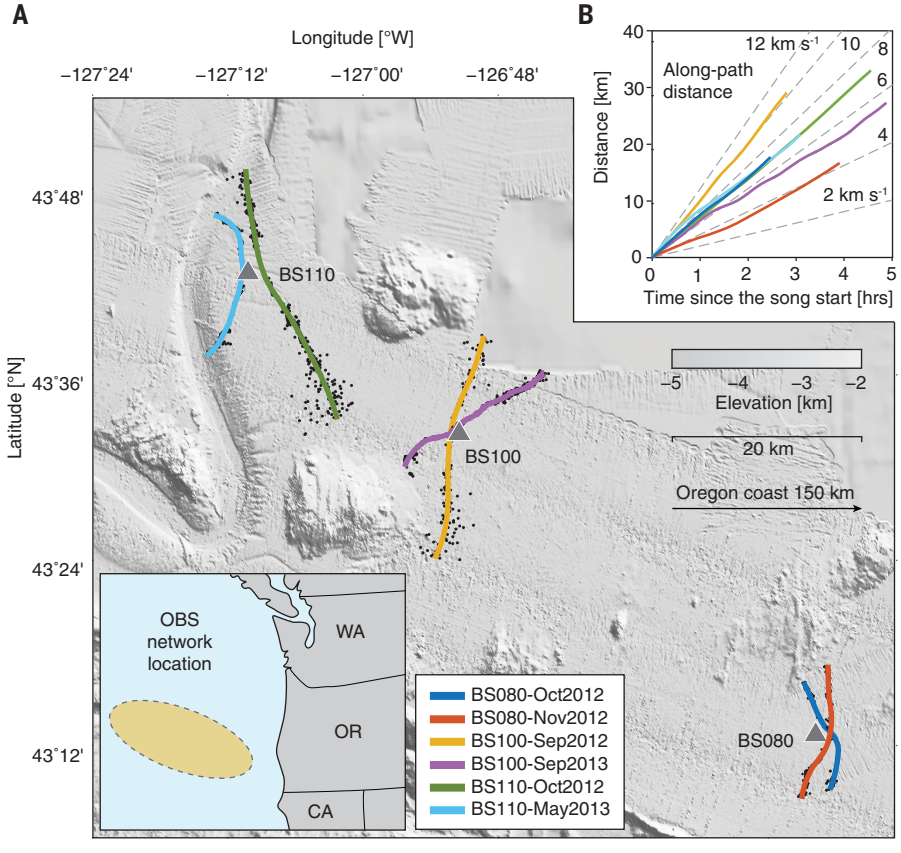

Fig. 2. Analyzed whale songs and travel paths. (**A**) Seafloor bathymetry, station location, and the whale travel path during the analyzed songs. Black dots denote location of individual calls, colored lines are smoothed whale travel paths, and gray triangles represent stations. The orientation map on the bottom left shows the OBS network location in the northeast Pacific. (**B**) Source-station offset plotted as a function of time elapsed since the beginning of the song.

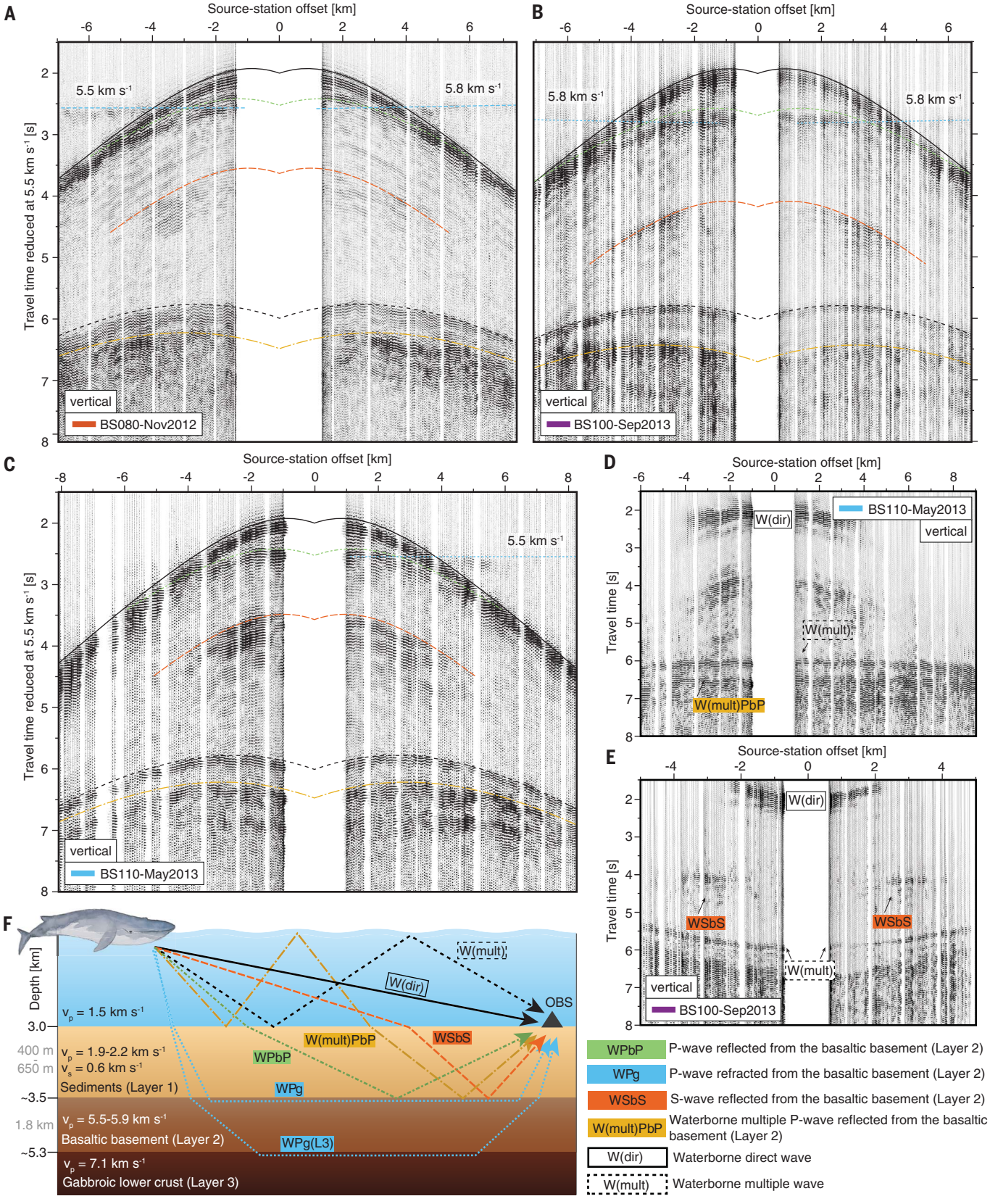

Fig. 3. Interpreted song gathers from stations BS080, BS100, and BS110. (**A** to **C**) Song gathers with identified phase travel times (A) BS080-Nov2012, (B) BS100-Sep2013, and (C) BS110-Oct2012. The theoretical phase travel times (colored lines) are based on the seismic velocities and layer thicknesses given in the main text and Table 1. (**D** and **E**) Optimal NMO correction that flattens the (D) W(mult)PbP phase arrival at BS110-May2013 and (E) WSbS phase arrival at BS100-Sep2013. (**F**) Model of the upper oceanic crust, with seismic velocities and ray paths. The model depth is not to scale.

Table 1. Crustal seismic velocities and layer thicknesses with 95% uncertainty intervals estimated from individual song gathers. A "–" indicates parameters that could not be estimated from the song gather.

		Layer 1			Layer 2			Layer 3
		Seismic velocity (km s^{-1})			*P*-wave velocity (km s^{-1})			
OBS station	**Song ID**	*P*-wave velocity based on W(mult)PbP NMO correction	*S*-wave velocity based on WSbS NMO correction	**Layer thickness (m)**	Based on WPg - north arrival time	Based on WPg - south arrival time	**Layer thickness (km) based on WPg(L3) intercept time**	***P*-wave velocity (km s^{-1}) based on WPg(L3) arrival time**
BS080	BS080-Oct2012	2.2 ± 0.4	0.6 ± 0.1	490 ± 40	–	–	–	–
	BS080-Nov2012	2.1 ± 0.1	–	510 ± 130	5.5 ± 0.2	5.8 ± 0.2	–	–
BS100	BS100-Sep2012	2.0 ± 0.1	–	660 ± 30	–	–	–	–
	BS100-Sep2013	2.1 ± 0.1	0.6 ± 0.1	650 ± 60	–	–	–	–
BS110	BS110-Oct2012	2.0 ± 0.2	–	380 ± 60	5.9 ± 0.1	–	1.8 ± 0.3	7.1 ± 0.1
	BS110-May2013	1.9 ± 0.1	0.6 ± 0.1	400 ± 30	5.5 ± 0.3	–	–	–
Overall	–	1.9 to 2.2	0.6	380 to 650	5.5 to 5.9		1.8 ± 0.3	7.1 ± 0.1

that results from the uncertainty in the whale dive depth is negligible (~0.2%). The BS110-Oct2012 song gather displays WPg arrival up to 19-km offset south of the station (figs. S8 and S12). At offsets larger than 12 km, the phase arrivals suggest that velocity increases to roughly 7.1 ± 0.1 km s^{-1}, which is in agreement with the oceanic layer 3. With this result, the estimated thickness of layer 2 is 1.8 ± 0.3 km. The station BS110 (fig. S8) shows particularly well the direct, reflected, and converted phases that constrain the derived crustal model.

Our results with uncertainties conform to the archetypal structure of the oceanic crust, where the gabbroic lower crust (layer 3) is overlain by extrusive basalts (layer 2) and unconsolidated, hydrated sediments (layer 1) (*23*). A seismic image derived from a controlled-source transect about 200 km north of the studied site (*24*) indicates a sediment thickness of roughly 700 to 800 m. At the Blanco fault zone sites, the sediments are 100 to 300 m thinner, which may be due to the sites' greater distance from the sediment sources in the Columbia River estuary and the Juan de Fuca Strait. Our estimates of the sediment v_p/v_s ratio are lower than those suggested by the controlled-source experiment (*25*) farther north, indicating sediment over-compaction, which may have occurred because of the proximity to the Blanco fault and repeated exposure to strong earthquake shaking (*26*). The basaltic basement (layer 2) thickness and the *P*-wave velocity match values observed for this layer of the same crustal age, and the *P*-wave velocity of layer 3 falls within the globally observed range (*23*).

The three studied sites show consistent results, congruent with regional and global observations, and demonstrate that fin whale calls can be used for seismic imaging of the oceanic crust. This method provides lower resolution than air-gun surveys, owing to the narrower frequency band and lower dominant frequency of fin whale calls. Higher-pitch whale vocalizations with a broader frequency band, such as those of sperm whales, could be used for high-resolution studies of the ocean-floor sediments. The source location procedure (*20*) used here limits the application to relatively flat regions without substantial bathymetrical features. Regions of high topography and crustal heterogeneity would require a more sophisticated three-dimensional approach and source location based on multiple seismic stations. We suggest that machine-learning algorithms, such as deep neural networks, could be used for automatic whale location and song processing.

Although fin whale vocalizations do not have the potential to replace high-energy broadband air-gun signals in ocean crust studies, they may complement passive seismic experiments during deployments of ocean-bottom seismic stations. More generally, our study demonstrates that animal vocalizations are useful not only for studying the animals themselves but also for investigating the environment that they inhabit.

REFERENCES AND NOTES

1. J. V. Carretta *et al*., "U.S. Pacific Marine Mammal Stock Assessments: 2013" (NOAA Technical Memorandum NMFS, NOAA-TM-NMFS-SWFSC-532, NOAA, 2014).
2. A. Aguilar, in *Encyclopedia of Marine Mammals*, W. F. Perrin, Ed. (Elsevier, 2008), pp. 433–436.
3. J. G. Cooke, *Balaenoptera physalus*. The IUCN Red List of Threatened Species 2018: e.T2478A50349982 (2019); https://dx.doi.org/10.2305/IUCN.UK.2018-2.RLTS.T2478A50349982.en.
4. W. J. Richardson, C. R. Greene Jr., C. I. Malme, D. H. Thomson, *Marine Mammals and Noise* (Academic Press, 2013).
5. A. Širović, J. A. Hildebrand, S. M. Wiggins, *J. Acoust. Soc. Am.* **122**, 1208–1215 (2007).
6. M. J. Weirathmueller, W. S. D. Wilcock, D. C. Soule, *J. Acoust. Soc. Am.* **133**, 741–749 (2013).
7. W. A. Watkins, P. Tyack, K. E. Moore, J. E. Bird, *J. Acoust. Soc. Am.* **82**, 1901–1912 (1987).
8. M. A. McDonald, J. A. Hildebrand, S. C. Webb, *J. Acoust. Soc. Am.* **98**, 712–721 (1995).
9. S. A. Mizroch, D. W. Rice, D. Zwiefelhofer, J. Waite, W. L. Perryman, *Mammal Rev.* **39**, 193–227 (2009).
10. M. Simon, K. M. Stafford, K. Beedholm, C. M. Lee, P. T. Madsen, *J. Acoust. Soc. Am.* **128**, 3200–3210 (2010).
11. W. S. D. Wilcock, *J. Acoust. Soc. Am.* **132**, 2408–2419 (2012).
12. R. Iwase, *Jpn. J. Appl. Phys.* **54**, 07HG03 (2015).
13. O. Gaspà Rebull, J. Díaz Cusí, M. Ruiz Fernández, J. Gallart Muset, *J. Acoust. Soc. Am.* **120**, 2077–2085 (2006).
14. W. A. Watkins, *Sci. Rep. Whales Res. Inst.* **33**, 83–117 (1981).
15. D. C. Soule, W. S. Wilcock, *J. Acoust. Soc. Am.* **133**, 1751–1761 (2013).
16. M. J. Weirathmueller *et al*., *PLOS ONE* **12**, e0186127 (2017).
17. J. L. Nábělek, J. Braunmiller, Plate boundary evolution and physics at an oceanic transform fault system. International Federation of Digital Seismograph Networks (2012); https://doi.org/10.7914/SN/X9_2012.
18. V. M. Kuna, J. L. Nábělek, J. Braunmiller, *Nat. Geosci.* **12**, 138–142 (2019).
19. D. S. Wilson, *J. Geophys. Res. Solid Earth* **98**, 16053–16071 (1993).
20. Materials and methods are available as supplementary materials.
21. A. K. Stimpert *et al*., *Anim. Biotelem.* **3**, 23 (2015).
22. C. A. Zelt, R. B. Smith, *Geophys. J. Int.* **108**, 16–34 (1992).
23. G. L. Christeson, J. A. Goff, R. S. Reece, *Rev. Geophys.* **57**, 504–529 (2019).
24. G. Horning *et al*., *J. Geophys. Res. Solid Earth* **121**, 5859–5879 (2016).
25. J. Zhu *et al*., *J. Geophys. Res. Solid Earth* **125**, e2019JB019239 (2020).
26. D. E. Sawyer, J. R. DeVore, *Geophys. Res. Lett.* **42**, (2015).
27. J. L. Nábělek, R/V Melville, cruise MV1212. R2R (2012); http://dx.doi.org/10.7284/902871.

ACKNOWLEDGMENTS

We thank K. Davenport for assistance with data processing, T. Kudrnova for the whale illustration used in Figs. 1 and 3, and S. Gyles for reviewing the manuscript. Comments by A. Trehu and J. Braunmiller improved the rigor of the paper. **Funding:** The seismic stations for the project were provided by the U.S. Ocean Bottom Seismograph Instrument Pool (www.obsip.org), funded by the National Science Foundation (NSF). This research was supported by NSF grants OCE-1031858 and OCE-1131767. **Author contributions:** J.L.N. collected the dataset. V.M.K. conducted the data analysis. Both authors discussed the results and contributed to writing the manuscript. **Competing interests:** The authors declare no competing financial interests. **Data and materials availability:** The OBS dataset is archived at the IRIS Data Management System (www.iris.edu) under network code X9 for the Plate Boundary Evolution and Physics at an Oceanic Transform Fault System project (*17*). Raw bathymetry data, used in Fig. 2 and for whale location, are available from the Rolling Deck to Repository (R2R), R/V Melville, cruise MV1212 (*27*).

SUPPLEMENTARY MATERIALS

science.sciencemag.org/content/371/6530/731/suppl/DC1
Materials and Methods
Supplementary Text
Figs. S1 to S12
Table S1
References (*28*–*30*)

23 October 2020; accepted 5 January 2021
10.1126/science.abf3962

Seismic crustal imaging using fin whale songs

Václav M. Kuna and John L. Nábelek

Science **371** (6530), 731-735.
DOI: 10.1126/science.abf3962

Structure from a whale song

Probing the structure of the ocean crust requires a wave source. The most common source is an air gun, which is effective but potentially harmful for ocean life and not easy to use everywhere. Kuna and Nábelek found that fin whale songs can also be used as a seismic source for determining crustal structure. Fin whale vocalizations can be as loud as large ships and occur at frequencies useful for traveling through the ocean floor. These properties allow fin whale songs to be used for mapping out the density of ocean crust, a vital part of exploring the seafloor.

Science, this issue p. 731